ACS APPLIED ELECTRONIC MATERIALS

Article

Cite This: ACS Appl. Electron. Mater. 2019, 1, 2619−2625

pubs.acs.org/acsaelm

Origin of Band Modulation in GeTe-Rich Ge−Sb−Te Thin Film

Deniz P. Wong,[*,†,¶,◐] Masoud Aminzare,[†,◐] Ta-Lei Chou,[†] Chin-Sheng Pang,[‡] Yi-Ren Liu,[‡] Tzu-Hsien Shen,[†] Benjamin K. Chang,[†] Hsiang-Ting Lien,[‡] Sun-Tang Chang,[∥] Chia-Hua Chien,[⊥] Yang-Yuan Chen,[⊥] Ming-Wen Chu,[‡,§] Yaw-Wen Yang,[∥] Wen-Pin Hsieh,[#] Gerda Rogl,[▽,○] Peter Rogl,[▽,○] Yohei Kakefuda,[◆] Takao Mori,[◆] Mei-Yin Chou,[†] Li-Chyong Chen,[*,‡,§] and Kuei-Hsien Chen[*,†,‡]

[†]Institute of Atomic and Molecular Sciences, Academia Sinica, Taipei 10617, Taiwan

[‡]Center for Condensed Matter Sciences, National Taiwan University, Taipei 10617, Taiwan

[§]Center of Atomic Initiative for New Materials, National Taiwan University, Taipei 10617, Taiwan

[∥]National Synchrotron Radiation Research Center, Hsinchu 30076, Taiwan

[⊥]Institute of Physics, Academia Sinica, Taipei 11529, Taiwan

[#]Institute of Earth Sciences, Academia Sinica, Taipei 11529, Taiwan

[▽]Christian Doppler Laboratory for Thermoelectricity, Institute of Materials Chemistry, University of Vienna, Währingerstrasse 42, A-1090 Wien, Austria

[○]Institute of Solid State Physics, TU-Wien, Wiedner Hauptstrasse 8-10, A-1040 Wien, Austria

[◆]International Center for Materials Nanoarchitectonics (WPI-MANA) and Center for Functional Sensor & Actuator (CFSN), Namiki 1-1, Tsukuba 305-0044, Japan

Supporting Information

ABSTRACT: Germanium tellurides and their pseudobinary compounds offer interesting properties that are important in thermoelectric and phase-change applications. Despite being a class of materials under scrutiny since its discovery, unique properties and functionalities have kept on emerging in recent years. In this work, we observed another unique property of Ge−Sb−Te (GST) thin film that can be beneficial in its development for thermoelectric applications. A rapid heating and quenching process of the GST film resulted in a metastable rock-salt cubic structure, exhibiting a unique electronic-transition-like behavior. Above the transition temperature at 150 °C, we observed a temperature-induced band modulation, corroborated with changes in its effective mass and valence band position that leads to favorable electronic and thermoelectric properties. Charge transfer between Sb and Te occurred, accompanied by a distorted cubic-to-cubic structural change. The interplay of the electronic and lattice structure born out of the composition and phase of the Ge−Sb−Te thin film opened up the possibility for the future of thermoelectric devices.

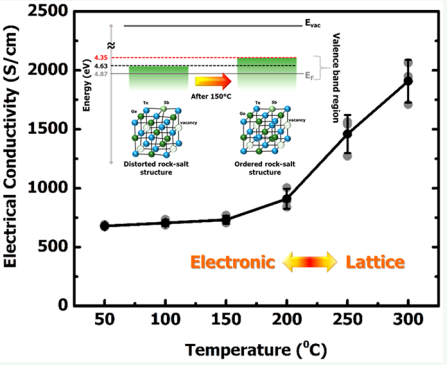

KEYWORDS: *band modulation, electronic transition, germanium tellurides, phase-change, thermoelectric*

INTRODUCTION

Germanium tellurides and their pseudobinary counterparts have long been used in electronic-related devices. Specifically, the report of S. R. Ovshinsky in 1968[1] on a semiconductor behavior that can easily cross-over between a highly resistive state and a conducting state has placed this class of materials under the scrutiny of various scientific curiosities about its properties and functionalities. Ge−Sb−Te (GST) has garnered most of its prominence in phase-change memory applications such as optical storage devices and memory devices.[2−6] Recently, its applications extended into photonics,[7,8] plasmonics,[9] and even thermoelectric applications.[10,11]

The increasing possibilities of this class of material have motivated many scientists to continue to study and understand the underlying properties it can exhibit.[12] Most of the thermoelectric studies for GST-related compounds focused on bulk systems with the highest reported zT value of about 2.4.[13−17] In the case of bulk compounds, its thermoelectric properties are tunable by varying composition,[18] microstructure,[19] and vacancy content.[20] The highest thermoelectric performance occurs when the material is GeTe-rich in

Received: September 13, 2019
Accepted: November 19, 2019
Published: November 19, 2019

DOI: 10.1021/acsaelm.9b00596
ACS Appl. Electron. Mater. 2019, 1, 2619−2625

composition and transforms into its higher-temperature rock-salt cubic structure.[21−23] This phase is interesting because, in addition to possessing a higher thermoelectric performance, thin films of a GeTe-rich GST phase also stabilize in this cubic state even at room temperature.[24,25] The stark contrast between the bulk and thin-film form of this compound motivated us to look into the latter form for a possible enhancement in its thermoelectric properties.

The variation between the bulk and thin-film version of the same compound is not something surprising. Due to the fabrication process, different microstructures can form from varying nucleation and growth processes.[26] Furthermore, the presence of another interface such as the substrate contributes an additional external effect creating possible strain and a varying mass diffusion process.[27,28] Earlier reports on the thermoelectric studies of GST films have shown promise in achieving a better thermoelectric performance compared to the reported bulk counterparts at the same operating temperature range. However, these works investigated only a narrow operating temperature range.[29] In contrast, our current work showed that, by going beyond this temperature, we observed a unique transition temperature, albeit with appropriate process conditions, which can improve its electrical conductivity without sacrificing its Seebeck coefficient. Recent studies on GST systems have suggested a disorder−order transformation-induced vacancy ordering, consequently influencing their electronic properties.[30−32] Although it is still debatable, our current work demonstrated that such electronic-transition-like phenomena can ultimately lead to an improved thermoelectric performance. The accompanying in situ observation of the lattice and electronic structure at the transition temperature gave strong evidence on the possible origins of such band modulation.

RESULTS AND DISCUSSION

Previously, we also have shown that the thermoelectric properties of GST in the thin-film form were tunable through morphological control and different from its bulk counterpart.[33] Here, we further demonstrate that a nonequilibrium thermal treatment, in which the film was rapidly heated (at a rate of ∼50 °C/min) up to its decomposition temperature (∼550 °C) followed immediately by fast air-quenching, allowed us to obtain a nonstoichiometric GeTe-rich GST thin film. The quenching process is needed to maintain stability of the film otherwise the interdiffusion of the Sb and Te elements as reported by Lee et al.[34] causes significant modification to the film structure and composition. The process allowed us to maintain the initial composition within our measurement temperature region (Figure S1). After obtaining the crystalline phase through this process, no additional or changed structural phase was observed (Figure S2). All the diffraction peaks can be identified as rock-salt cubic structure with no rigorously defined phase transition. Furthermore, there is no sign of significant preferred orientation of the film, and the small crystallite size (40 nm) calculated based from the Scherrer equation suggests that the film is polycrystalline in nature and that a similar electronic and thermal transport behavior in both the in-plane and out-of-plane direction would be expected.

Looking at the temperature-dependent thermoelectric parameter values, the improved performance comes from a number of favorable conditions such as a rapid increase in electrical conductivity (Figure 1a) while keeping a relatively

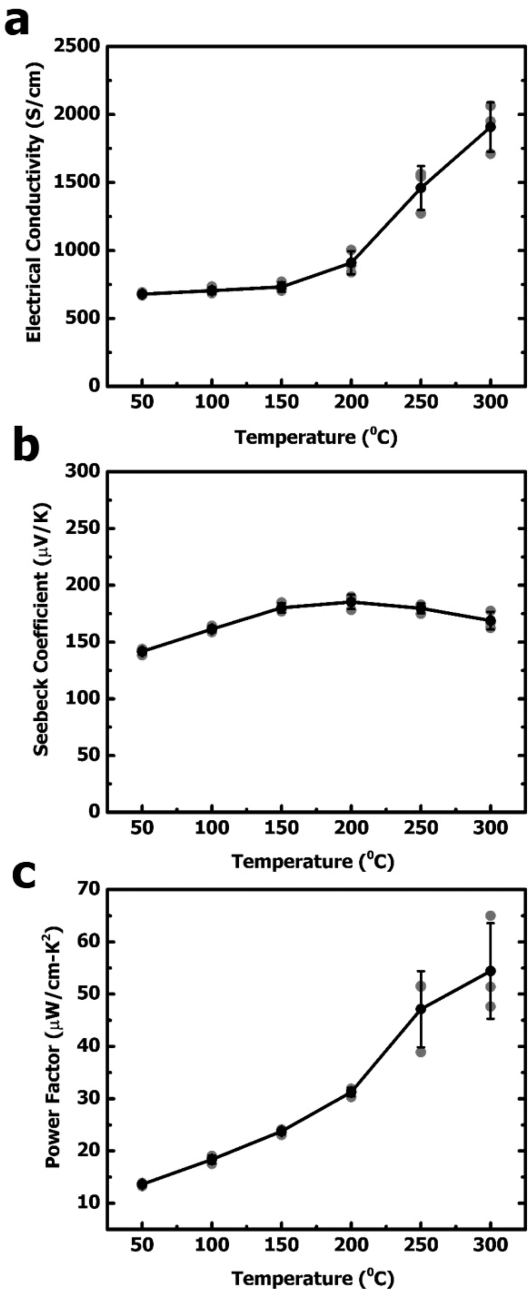

Figure 1. Thermoelectric properties as a function of temperature for Ge−Sb−Te thin films. (a) Electrical conductivity. (b) Seebeck coefficient. (c) Power factor.

temperature-independent high Seebeck coefficient (Figure 1b) above 150 °C. This allowed us to obtain an average power factor around 54 (±9) μW/cm K (Figure 1c). A high value of the power factor indicates that a TE device with this material can extract more energy from the temperature gradient generated. We also corroborated our measurements from another group using their own ZEM-3 system (Figure S3) and obtained agreeable results. At the same time, a similar trend was also achievable on a different sample with varied composition (Figure S4). To evaluate the contribution from the substrate, measurement on a blank substrate was carried out as well (Figure S5). As revealed by the negative Seebeck coefficient, the intrinsic Si substrate carries *n*-type carriers with very low electrical conductivity consistent with the reported

DOI: 10.1021/acsaelm.9b00596
ACS Appl. Electron. Mater. 2019, 1, 2619−2625

behavior.[35] Thus, this unique electronic feature can be attributed solely to the GST film.

Applying the Arrhenius equation to the temperature-dependent electrical conductivity data, two activation energies can clearly be distinguished below and above the transition temperature (Figure 2a). The activation energy observed above the transition temperature is higher compare to its lower counterpart plausibly due to different types of operating carriers and can be attributed to a heavy-hole carrier typically generated in high-zT thermoelectric materials at a higher temperature as reported by Biswas et al.[36] In order to confirm this behavior, we performed a temperature-dependent Hall measurement on the sample to determine the Hall coefficient (Figure S6), carrier concentration, mobility, and effective mass (Figure 2b). The rapid change in all these physical parameters above the transition point can be attributed to the contribution of another band as observed by Wu et al. on the bulk GeTe-based system.[37] This phenomenon was observed throughout different batches of samples (Figure S7). The temperature-dependent effective mass, m^*, was obtained using eq 1:

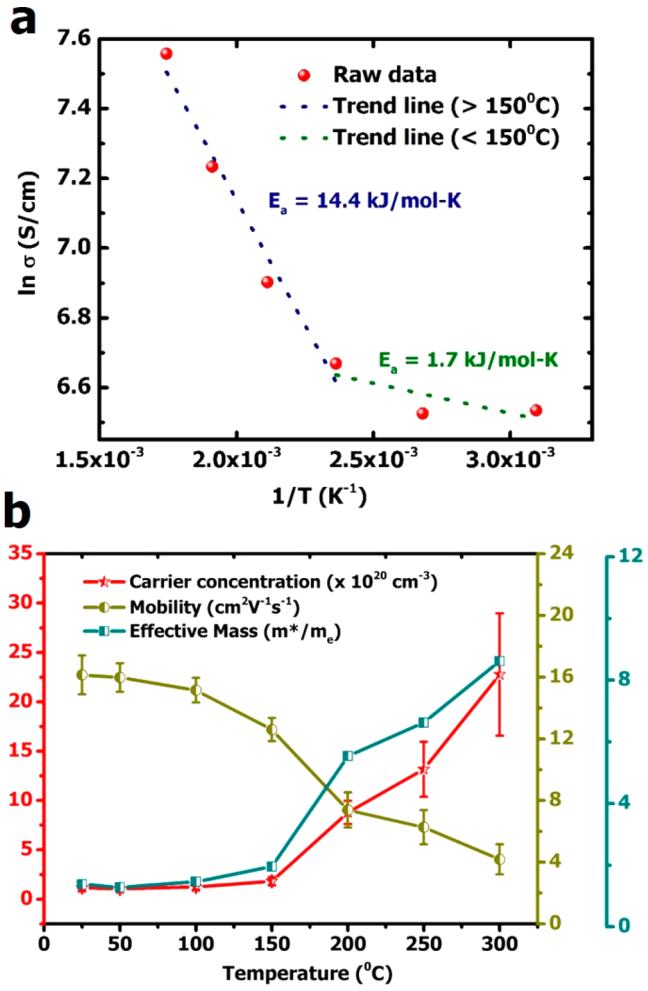

Figure 2. Electronic transport properties of Ge−Sb−Te thin films. (a) Arrhenius plot of electrical conductivity. (b) Carrier concentration, mobility, and effective mass.

$$S = \frac{8\pi^2 K_B^2}{3eh^2} m^* T \left(\frac{\pi}{3\eta}\right)^{2/3} \quad (1)$$

where S stands for the Seebeck coefficient, K_B is the Boltzmann constant, e is the elementary charge, h is Planck's constant, m^* is the effective mass, T is the temperature in Kelvin, and η is the carrier concentration. Notably, an abrupt multifold increase in the effective mass was observed above 150 °C, which implies certain temperature-induced modulation in the band structure, similar to the band convergence phenomenon reported by Pei et al.[38] and Liu et al.[39] occurring in a different but high-performance thermoelectric material system.

In order to investigate the origins of the temperature evolution of the energy levels, we performed a temperature-dependent photoelectron spectroscopy study on the film. Ultraviolet photoelectron spectroscopy (UPS) allows us to probe the valence band region and work function of the material. In contrast, X-ray photoelectron spectroscopy (XPS) allows us to probe the core-level region and observe the chemical and electronic states of the elements within the material. The valence band spectra of Ge−Sb−Te observed in Figure 3a contain two peaks around 0.75 and 2.75 eV. These are consistent features attributed to Ge 4p, Sb 5p, and Te 5p orbitals of Ge−Sb−Te as demonstrated by Kim et al.[40] Moreover, by obtaining temperature-dependent spectra, Figure 3a shows a shift in the valence band maximum of about 0.25 eV toward the vacuum level when heated above 150 °C (transition temperature). The upshift of the valence band is consistent with the generation of the second carrier above the transition temperature and indicates a plausible convergence of band in the material. Most reported band convergence phenomena occur when the chemical structure is tunable by doping or alloying,[41] whereas we observed a temperature-induced band convergence-like behavior in Ge−Sb−Te above a transition temperature of 150 °C. The directly measured shift in the valence band by UPS, together with the aforementioned change in the effective mass, concertedly implies a valence band modulation, allowing the material to gain access to the electronic state from another band below its original valence band position as shown from ab initio calculations (Figure S8). The ground-state band structure of the GeTe crystal containing both a Ge vacancy and a Sb atom substituting a nearest-neighbor Ge atom in a 4 × 4 × 4 supercell has suggested no significant change in the band dispersions. The temperature-dependent band structure calculation is still not possible at the present time. The full-scale UPS spectra (Figure S9) show that there are no significant changes in our work function; thus, the temperature-dependent band modulation can be attributed to the changes observed in the valence band region.

Furthermore, XPS data (Figure S10) have shown no changes in the germanium peak while a shift toward the lower binding energy was notable for the tellurium peaks and a higher binding energy for the antimony peaks. To get a better peak quality, the Sb 3d and Te 3d peaks (Figure S11) were also obtained, and a similar trend was observed (Figure 3b,c), suggesting a charge transfer effect between Sb and Te. The occurrence of the shift in these two peaks also coincides with that of the transition temperature observed in electrical conductivity. Such an effect causes the changes in the electronic transition as observed in the band structure, consequently, the increase in the power factor. The resonant bonding model, used to describe the local structure of the GST system[42] also reinforces the plausibility of a delocalization of electrons through the alignment of the p-orbital between the Sb and Te atoms.[43,44]

DOI: 10.1021/acsaelm.9b00596
ACS Appl. Electron. Mater. 2019, 1, 2619−2625

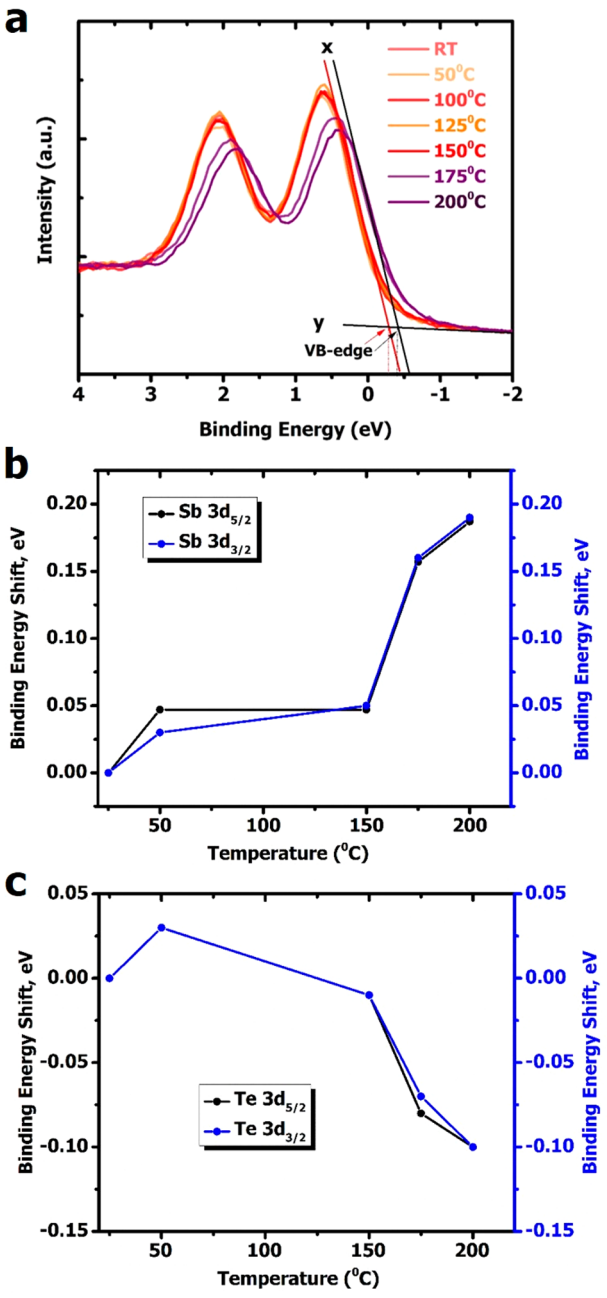

Figure 3. Photoemission spectroscopy as a function of temperature for Ge−Sb−Te thin films. (a) Temperature-dependent valence band spectra and work function using an excitation energy of 40 eV. The energy positions at the valence band edge were taken to be the intersection points of the fitted lines labeled "x" and "y" on the spectrum. (b) XPS binding energy shift obtained from Sb 3d (Figure S10a,b). (c) XPS binding energy shift obtained from Te 3d (Figure S10c,d).

Besides observing the changes in the electronic structure of the material, we also monitored the structural evolution near the transition temperature. Despite no change in the phase present, apparent red shifts in peak positions and, therefore, an increase in the corresponding lattice constants (Figure 4) were observed. This can also be supported by the changes in the temperature-dependent selected area electron diffraction (SAED) obtained from our TEM analysis (Figure S12). It should be emphasized that, by comparing with known thermal

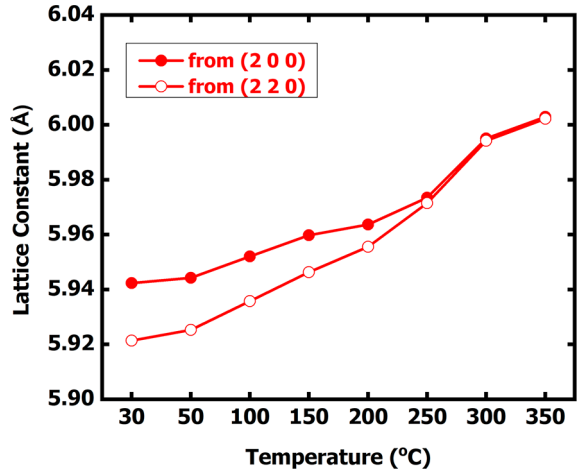

Figure 4. Lattice constant as a function of temperature of Ge−Sb−Te film obtained from the XRD pattern calculated using the (2 0 0) and (2 2 0) position.

expansion coefficients from related materials, the noteworthy lattice expansion observed in our GST thin film does not follow the thermal expansion coefficients of the bulk GeTe or $Ge_2Sb_2Te_5$ materials, or the substrates (Figure S13), of which the changes are negligible over the temperature range of interest. However, as we scratched the GST from the substrate and performed the temperature-dependent XRD measurement on the powdered sample, we observed an almost similar behavior to the bulk system. This unusual behavior of the GST thin film continues to persist as observed from the disparity of lattice constants at room temperature calculated from different orientations. This is in contrast to most known cubic structures and with the powdered sample obtained from the scratched film (Figure S14). With increasing temperature, specifically above the transition temperature, the lattice constant values converged, indicating an ordering of the crystal structure. It is known from the literature that the rock-salt cubic structure is a high-temperature phase, and such a structure can be sustained down to lower temperatures in a metastable distorted form.[45] With a further increase of the temperature, a perfect cubic transformation was observed, with the same lattice constant values calculated from two different crystal orientations (200 and 220). Furthermore, this effect is reversible as indicated by the lattice constants obtained from several heating and cooling cycles (Figure S15). This slight structural transformation may induce strain energy in the material system that leads to changes in its electronic properties.[46] Similarly, by observing the evolution of the film in situ under the electron microscope, we observed the presence of a stacking fault that typically is present for a cubic system such as GST (Figure S16). The slight movement of the stacking fault might influence the local chemical environment and lead to a considerable increase in the electrical conductivity of the film.[47]

For the first time, by monitoring both the structural and electronic structures of the film at the measured temperature range, we were able to observe the possible origins of the band modulation wherein a distorted-to-order structure was observed that causes a charge transfer effect between the Sb and Te. The transition caused by such phenomena allowed the sudden increase in our film's electrical conductivity thus boosting further its power factor and consequently plausibly its zT value. Such observation opens up an avenue of further

DOI: 10.1021/acsaelm.9b00596
ACS Appl. Electron. Mater. 2019, 1, 2619−2625

development for this class of material in the future and offers insight into a different origin of electronic band modification.

CONCLUSION

The temperature-induced structural ordering leading band modulation of the GST thin film has shown a unique property that can boost the thermoelectric performance. Without observing any phase change, we have demonstrated that, above 150 °C, the band modulation leads to favorable thermoelectric parameters. In this transition state, we also observed a charge transfer between the antimony and tellurium atoms and in parallel a distorted cubic to an ordered cubic transformation. These findings not only provide intriguing information on the known phase-change characteristics but also give new perspectives for the thermoelectric properties of Ge−Sb−Te and the development of new functional nanodevices.

EXPERIMENTAL METHODS

Thin-Film Fabrication. Ge−Sb−Te thin films were deposited on intrinsic single crystal ⟨100⟩ Si substrates (electrical resistivity ≥3000 Ω cm, Semiconductor Wafers, Inc.) using a radiofrequency magnetron sputtering system, with a base pressure $<10^{-6}$ Torr. Commercial 2 in. $Ge_{19}Sb_2Te_{22}$ target (99.9%, Toshima, Japan) was used for this study. Before deposition, the Si substrates were cleaned using a standard RCA process. The target was kept facing the substrate holder ≈12 cm away. In order to deposit uniform films, the substrate was rotated with a fixed speed throughout the deposition. Sputter-etches of 5−10 min were used to remove the target surface contaminations. The target power, argon flow rate, and working pressure were fixed at 80 W, 2 sccm, and 1.3 mTorr, respectively. The deposition time was 18 min, and the resulting film thickness was approximately 250−300 nm, estimated from scanning electron microscopy (SEM, JEOL JSM-6700F) cross-section images. The as-deposited film has an amorphous feature and requires a postannealing treatment, by heating to 550 °C at a heating rate of 50 °C/min under Ar atmosphere without holding time. The plan-view and cross-section images of the film are available in the Supporting Information (Figure S17).

Electrical Transport Properties. The temperature-dependent electrical conductivity and Seebeck coefficient were obtained with the commercial ZEM-3 system by ULVAC using a special thin-film holder. Typical thin-film samples used for these measurements were cut into 10 mm × 3 mm slivers. Temperature-dependent Hall effect measurements (to obtain carrier concentration and mobility) were obtained with the commercial ECOPIA HMS-3000. The sample used for these measurements had the size of about 15 mm × 15 mm.

Structural and Composition Characterizations. The compositions, as summarized in Table S1, were checked using an electron probe microanalyzer (EPMA), or wavelength-dispersive spectroscopy (WDS), attached to an SEM (JEOL JXA-8200 Electron Probe X-ray microanalyzer) and confirmed by inductively coupled plasma optical emission spectrometry (ICP-OES, Agilent 725) and X-ray photoelectron spectroscopy (XPS, NSRRC BL024A).

Structural analysis was done using temperature-dependent XRD (Pananalytical Empyrean) with Cu $K\alpha_1$ radiation (λ = 0.154 nm). A heating stage inside the X-ray diffractometer controls the temperature from room temperature to 350 °C with an increment of 50 °C for each measurement. Temperature-dependent changes in the lattice constant through the selected area electron diffraction (SAED) were crosschecked using a transmission electron microscope (JEOL, JEM-2100) equipped with a heating stage.

Synchrotron-Based Study. Photoemission spectroscopy was performed in the National Synchrotron Radiation Research Center (NSRRC), Hsinchu, Taiwan, at beamline 24A. This beamline offers a 1.5 GeV bending magnet in a wide range spherical grating monochromator based on the Dragon type design giving a photon flux of 1×10^{10} to 5×10^{11} photons/s. The samples were loaded in a heating stage and evacuated to a base pressure of 1×10^{-9} Torr. Prior to data acquisition, an Ar ion-sputtering gun was used to clean the sample surface by removing oxides and unwanted substances. For the ultraviolet photoemission spectroscopy (UPS), the electron energy was measured with a PHOIBOS 150 energy analyzer (SPECS GmbH) equipped with a charge-coupled device detector housed in a magnetically shielded mu-metal chamber. The UPS excitation energy was 40 eV, and the Fermi edge was calibrated to a cleaned Mo surface. The total energy resolution was estimated from the Fermi cutoff of the Mo surface to be 100−200 meV at room temperature (RT) depending on the experimental conditions. A sample bias of −5.0 V was applied during the measurements in order to distinguish between the analyzer and the sample cutoffs for work function determination. For the X-ray photoemission study, an excitation energy of 750 eV was used. Similarly, the sample surface was cleaned prior to the experiment. The temperature-dependent component of the instrument used a resistive-heating function, and the temperature was monitored using a thermocouple attached to a digital thermometer (accuracy of ±10 °C).

Computational Methods. First-principles calculations were performed to investigate the electronic structure of a GeTe crystal in the presence of Ge vacancies and/or Sb substitution. Different configurations in a 4 × 4 × 4 supercell containing a Ge vacancy and/or a Sb atom replacing Ge were considered. We used the Vienna ab initio simulation package (VASP)[48,49] code with projector augmented wave (PAW) pseudopotentials.[50,51] The generalized gradient approximation (GGA)[52] was used for the exchange-correlation functional, and a Γ-centered 3 × 3 × 3 *k*-mesh for the supercell was adopted. We first carried out volume-constrained structural relaxation to determine the atomic geometry and then performed self-consistent electronic calculations including spin−orbit coupling (SOC). To compare the band dispersions in the presence of Ge vacancies and/or Sb substitution with those in the perfect GeTe crystal, we used the zone-unfolding technique[53] as implemented in the BandUP[54−57] code to represent the calculated band structure obtained using the supercell back in the Brillouin zone of the primitive cell.

ASSOCIATED CONTENT

Supporting Information

The Supporting Information is available free of charge at https://pubs.acs.org/doi/10.1021/acsaelm.9b00596.

Sample compositions, additional temperature-dependent electronic transport properties and validation, Hall coefficient, carrier concentration, band structure from calculations, raw data of UPS and XPS, temperature-dependent TEM, comparison of lattice constants, and SEM images (PDF)

AUTHOR INFORMATION

Corresponding Authors

*Phone: +886 2 33665200. E-mail: deniz.wong@helmholtz-berlin.de.

*E-mail: chenlc@ntu.edu.tw.

*E-mail: chenkh@pub.iams.sinica.edu.tw.

ORCID

Deniz P. Wong: 0000-0001-7126-0019

Chin-Sheng Pang: 0000-0001-8347-4102

Peter Rogl: 0000-0002-7733-1612

Takao Mori: 0000-0003-2682-1846

Present Address

¶D.P.W.: Dept. of Methods for Characterization of Transport Phenomena in Energy Materials, Helmholtz-Zentrum Berlin für Materialien and Energie, D-14109 Berlin, Germany

DOI: 10.1021/acsaelm.9b00596
ACS Appl. Electron. Mater. 2019, 1, 2619−2625

Author Contributions

◐D.P.W. and M.A. contributed equally to this work.

Notes

The authors declare no competing financial interest.

■ ACKNOWLEDGMENTS

This work was supported by the Thermoelectric Project (AS-106-SS-A01) funded by Center for Sustainability Science, Academia Sinica. The authors also acknowledge the technical support provided by the Nano Core Facility of Academia Sinica, Taiwan.

■ REFERENCES

(1) Ovshinsky, S. R. Reversible Electrical Switching Phenomena in Disordered Structures. *Phys. Rev. Lett.* **1968**, *21*, 1450−1453.
(2) Zalden, P.; Siegert, K. S.; Rols, S.; Fischer, H. E.; Schlich, F.; Hu, T.; Wuttig, M. Specific Heat of $(GeTe)_x(Sb_2Te_3)_{1-x}$ Phase-Change Materials: The Impact of Disorder and Anharmonicity. *Chem. Mater.* **2014**, *26* (7), 2307−2312.
(3) Kao, K.-F.; Lee, C.-M.; Chen, M.-J.; Tsai, M.-J.; Chin, T.-S. Ga2Te3Sb5—A Candidate for Fast and Ultralong Retention Phase-Change Memory. *Adv. Mater.* **2009**, *21* (17), 1695−1699.
(4) Milliron, D. J.; Raoux, S.; Shelby, R. M.; Jordan-Sweet, J. Solution-phase deposition and nanopatterning of GeSbSe phase-change materials. *Nat. Mater.* **2007**, *6*, 352.
(5) Bruns, G.; Merkelbach, P.; Schlockermann, C.; Salinga, M.; Wuttig, M.; Happ, T. D.; Philipp, J. B.; Kund, M. Nanosecond switching in GeTe phase change memory cells. *Appl. Phys. Lett.* **2009**, *95* (4), 043108.
(6) Wuttig, M.; Yamada, N. Phase-change materials for rewriteable data storage. *Nat. Mater.* **2007**, *6*, 824.
(7) Wu, C.; Yu, H.; Li, H.; Zhang, X.; Takeuchi, I.; Li, M. Low-Loss Integrated Photonic Switch Using Subwavelength Patterned Phase Change Material. *ACS Photonics* **2019**, *6*, 87−92.
(8) Gholipour, B.; Piccinotti, D.; Karvounis, A.; MacDonald, K. F.; Zheludev, N. I. Reconfigurable Ultraviolet and High-Energy Visible Dielectric Metamaterials. *Nano Lett.* **2019**, *19*, 1643−1648.
(9) Gholipour, B.; Karvounis, A.; Yin, J.; Soci, C.; MacDonald, K. F.; Zheludev, N. I. Phase-change-driven dielectric-plasmonic transitions in chalcogenide metasurfaces. *NPG Asia Mater.* **2018**, *10*, 533−539.
(10) Schneider, M. N.; Rosenthal, T.; Stiewe, C.; Oeckler, O. From phase-change materials to thermoelectrics? *Z. Kristallogr.* **2010**, *225*, 463.
(11) Fahrnbauer, F.; Souchay, D.; Wagner, G.; Oeckler, O. High Thermoelectric Figure of Merit Values of Germanium Antimony Tellurides with Kinetically Stable Cobalt Germanide Precipitates. *J. Am. Chem. Soc.* **2015**, *137* (39), 12633−12638.
(12) Hong, M.; Zou, J.; Chen, Z.-G. Thermoelectric GeTe with Diverse Degrees of Freedom Having Secured Superhigh Performance. *Adv. Mater.* **2019**, *31*, 1807071.
(13) Li, J.; Zhang, X.; Chen, Z.; Lin, S.; Li, W.; Shen, J.; Witting, I. T.; Faghaninia, A.; Chen, Y.; Jain, A.; Chen, L.; Snyder, G. J.; Pei, Y. Low-Symmetry Rhombohedral GeTe Thermoelectrics. *Joule* **2018**, *2* (5), 976−987.
(14) Williams, J. B.; Morelli, D. T. Understanding the superior thermoelectric performance of Sb precipitated $Ge_{17}Sb_2Te_{20}$. *J. Mater. Chem. C* **2016**, *4* (42), 10011−10017.
(15) Sankar, R.; Wong, D. P.; Chi, C.-S.; Chien, W.-L.; Hwang, J.-S.; Chou, F.-C.; Chen, L.-C.; Chen, K.-H. Enhanced thermoelectric performance of GeTe-rich germanium antimony tellurides through the control of composition and structure. *CrystEngComm* **2015**, *17* (18), 3440−3445.
(16) Samanta, M.; Biswas, K. Low Thermal Conductivity and High Thermoelectric Performance in $(GeTe)_{1-2x}(GeSe)_x(GeS)_x$: Competition between Solid Solution and Phase Separation. *J. Am. Chem. Soc.* **2017**, *139* (27), 9382−9391.
(17) Perumal, S.; Roychowdhury, S.; Negi, D. S.; Datta, R.; Biswas, K. High Thermoelectric Performance and Enhanced Mechanical Stability of p-type $Ge_{1-x}Sb_xTe$. *Chem. Mater.* **2015**, *27* (20), 7171−7178.
(18) Rosenthal, T.; Schneider, M. N.; Stiewe, C.; Döblinger, M.; Oeckler, O. Real Structure and Thermoelectric Properties of GeTe-Rich Germanium Antimony Tellurides. *Chem. Mater.* **2011**, *23* (19), 4349−4356.
(19) Sankar, R.; Wong, D. P.; Chi, C.-S.; Chien, W.-L.; Hwang, J.-S.; Chou, F.-C.; Chen, L.-C.; Chen, K.-H. Enhanced thermoelectric performance of GeTe-rich germanium antimony tellurides through the control of composition and structure. *CrystEngComm* **2015**, *17* (18), 3440−3445.
(20) Xu, X.; Xie, L.; Lou, Q.; Wu, D.; He, J. Boosting the Thermoelectric Performance of Psuedo-Layered $Sb_2Te_3(GeTe)_n$ via Vacancy Engineering. *Adv. Sci.* **2018**, *5*, 1801514.
(21) Perumal, S.; Roychowdhury, S.; Negi, D. S.; Datta, R.; Biswas, K. High Thermoelectric Performance and Enhanced Mechanical Stability of p-type $Ge_{1-x}Sb_xTe$. *Chem. Mater.* **2015**, *27* (20), 7171−7178.
(22) Sun, J.; Mukhopadhyay, S.; Subedi, A.; Siegrist, T.; Singh, D. J. Transport properties of cubic crystalline $Ge_2Sb_2Te_5$: A potential low-temperature thermoelectric material. *Appl. Phys. Lett.* **2015**, *106* (12), 123907.
(23) Lee, J. K.; Oh, M. W.; Kim, B. S.; Min, B. K.; Lee, H. W.; Park, S. D. Influence of Mn on crystal structure and thermoelectric properties of GeTe compounds. *Electron. Mater. Lett.* **2014**, *10* (4), 813−817.
(24) Da Silva, J. L. F.; Walsh, A.; Lee, H. Insights into the structure of the stable and metastable $(GeTe)_m(Sb_2Te_3)_n$ compounds. *Phys. Rev. B: Condens. Matter Mater. Phys.* **2008**, *78* (22), 224111.
(25) Matsunaga, T.; Morita, H.; Kojima, R.; Yamada, N.; Kifune, K.; Kubota, Y.; Tabata, Y.; Kim, J. J.; Kobata, M.; Ikenaga, E.; Kobayashi, K. Structural characteristics of GeTe-rich GeTe−Sb_2Te_3 pseudobinary metastable crystals. *J. Appl. Phys.* **2008**, *103* (9), 093511.
(26) Ohring, M. Why are thin films different from the bulk? *Proc. SPIE* **1993**, *2114*, 2114 Laser-Induced Damage in Optical Materials..
(27) Schlom, D. G.; Chen, L.-Q.; Eom, C.-B.; Rabe, K. M.; Streiffer, S. K.; Triscone, J.-M. Strain Tuning of Ferroelectric Thin Films. *Annu. Rev. Mater. Res.* **2007**, *37*, 589−626.
(28) Saha, R.; Nix, W. D. Effects of the Substrate on the Determination of Thin Film Mechnical Properties by Nano-indentation. *Acta Mater.* **2002**, *50* (1), 23−38.
(29) Siegert, K. S.; Lange, F. R. L.; Sittner, E. R.; Volker, H.; Schlockermann, C.; Siegrist, T.; Wuttig, M. Impact of vacancy ordering on thermal transport in crystalline phase-change materials. *Rep. Prog. Phys.* **2015**, *78* (1), 013001.
(30) Zhang, W.; Thiess, A.; Zalden, P.; Zeller, R.; Dederichs, P. H.; Raty, J. Y.; Wuttig, M.; Blügel, S.; Mazzarello, R. Role of vacancies in metal−insulator transitions of crystalline phase-change materials. *Nat. Mater.* **2012**, *11*, 952.
(31) Wuttig, M.; Lüsebrink, D.; Wamwangi, D.; Wełnic, W.; Gilleßen, M.; Dronskowski, R. The role of vacancies and local distortions in the design of new phase-change materials. *Nat. Mater.* **2007**, *6*, 122.
(32) Siegrist, T.; Jost, P.; Volker, H.; Woda, M.; Merkelbach, P.; Schlockermann, C.; Wuttig, M. Disorder-induced localization in crystalline phase-change materials. *Nat. Mater.* **2011**, *10*, 202.
(33) Chen, I. N.; Chong, C.-W.; Wong, D. P.; Lyu, L.-M.; Chien, W.-L.; Anbalagan, R.; Aminzare, M.; Chen, Y.-F.; Chen, L.-C.; Chen, K.-H. Improving the thermoelectric performance of metastable rock-salt GeTe-rich Ge−Sb−Te thin films through tuning of grain orientation and vacancies. *Phys. Status Solidi A* **2016**, *213* (12), 3122−3129.
(34) Lee, E. K.; Lee, S.-Y. Thermal Stability and Microstructure of Germanium Antimony Telluride Thin Films under Interdiffusion Conditions. *Jpn. J. Appl. Phys.* **2018**, *57*, 081201.
(35) Fulkerson, W.; Moore, J. P.; Williams, R. K.; Graves, R. S.; McElroy, D. L. Thermal Conductivity, Electrical Resistivity, and

DOI: 10.1021/acsaelm.9b00596
ACS Appl. Electron. Mater. 2019, 1, 2619−2625

Seebeck Coefficient of Silicon from 100 to 1300 K. *Phys. Rev.* **1968**, *167* (3), 765−782.
(36) Biswas, K.; He, J.; Zhang, Q.; Wang, G.; Uher, C.; Dravid, V. P.; Kanatzidis, M. G. Strained endotaxial nanostructures with high thermoelectric figure of merit. *Nat. Chem.* **2011**, *3*, 160.
(37) Wu, D.; Zhao, L.-D.; Hao, S.; Jiang, Q.; Zheng, F.; Doak, J. W.; Wu, H.; Chi, H.; Gelbstein, Y.; Uher, C.; Wolverton, C.; Kanatzidis, M.; He, J. Origin of the High Performance in GeTe-Based Thermoelectric Materials upon Bi_2Te_3 Doping. *J. Am. Chem. Soc.* **2014**, *136* (32), 11412−11419.
(38) Pei, Y.; Shi, X.; LaLonde, A.; Wang, H.; Chen, L.; Snyder, G. J. Convergence of electronic bands for high performance bulk thermoelectrics. *Nature* **2011**, *473*, 66.
(39) Liu, W.; Tan, X.; Yin, K.; Liu, H.; Tang, X.; Shi, J.; Zhang, Q.; Uher, C. Convergence of Conduction Bands as a Means of Enhancing Thermoelectric Performance of *n*-Type $Mg_2Si_{1-x}Sn_x$ Solid Solutions. *Phys. Rev. Lett.* **2012**, *108* (16), 166601.
(40) Kim, J.-J.; Kobayashi, K.; Ikenaga, E.; Kobata, M.; Ueda, S.; Matsunaga, T.; Kifune, K.; Kojima, R.; Yamada, N. Electronic structure of amorphous and crystalline $(GeTe)_{1-x}(Sb_2Te_3)_x$ investigated using hard x-ray photoemission spectroscopy. *Phys. Rev. B: Condens. Matter Mater. Phys.* **2007**, *76* (11), 115124.
(41) Yin, K.; Su, X.; Yan, Y.; You, Y.; Zhang, Q.; Uher, C.; Kanatzidis, M. G.; Tang, X. Optimization of the Electronic Band Structure and the Lattice Thermal Conductivity of Solid Solutions According to Simple Calculations: A Canonical Example of the $Mg_2Si_{1-x-y}Ge_xSn_y$ Ternary Solid Solution. *Chem. Mater.* **2016**, *28* (15), 5538−5548.
(42) Shportko, K.; Kremers, S.; Woda, M.; Lencer, D.; Robertson, J.; Wuttig, M. Resonant bonding in crystalline phase-change materials. *Nat. Mater.* **2008**, *7*, 653.
(43) Huang, B.; Robertson, J. Bonding origin of optical contrast in phase-change memory materials. *Phys. Rev. B: Condens. Matter Mater. Phys.* **2010**, *81*, 081204R.
(44) Chen, N.-K.; Li, X.-B.; Wang, X.-P.; Tian, W. Q.; Zhang, S.; Sun, H.-B. Strong electron-polarized atom chain in amorphous phase-change memory Ge-Sb-Te alloy. *Acta Mater.* **2018**, *143*, 102−106.
(45) Matsunaga, T.; Kojima, R.; Yamada, N.; Kifune, K.; Kubota, Y.; Tabata, Y.; Takata, M. Single Structure Widely Distributed in a GeTe-Sb_2Te_3 Pseudobinary System: A Rock Salt Structure is Retained by Intrinsically Containing an Enormous Number of Vacancies within its Crystal. *Inorg. Chem.* **2006**, *45* (5), 2235−2241.
(46) Qin, G.; Yan, Q.-B.; Qin, Z.; Yue, S.-Y.; Cui, H.-J.; Zheng, Q.-R.; Su, G. Hinge-like structure induced unusual properties of black phosphorus and new strategies to improve the thermoelectric performance. *Sci. Rep.* **2015**, *4*, 6946.
(47) Li, X.-B.; Chen, N.-K.; Wang, X.-P.; Sun, H.-B. Phase-Change Superlattice Materials toward Low Power Consumption and High Density Data Storage: Microscopic Picture, Working Principles, and Optimization. *Adv. Funct. Mater.* **2018**, *28*, 1803380.
(48) Kresse, G.; Furthmüller, J. Efficiency of ab-initio total energy calculations for metals and semiconductors using a plane-wave basis set. *Comput. Mater. Sci.* **1996**, *6* (1), 15−50.
(49) Kresse, G.; Furthmüller, J. Efficient iterative schemes for ab initio total-energy calculations using a plane-wave basis set. *Phys. Rev. B: Condens. Matter Mater. Phys.* **1996**, *54* (16), 11169−11186.
(50) Blöchl, P. E. Projector augmented-wave method. *Phys. Rev. B: Condens. Matter Mater. Phys.* **1994**, *50* (24), 17953−17979.
(51) Kresse, G.; Joubert, D. From ultrasoft pseudopotentials to the projector augmented-wave method. *Phys. Rev. B: Condens. Matter Mater. Phys.* **1999**, *59* (3), 1758−1775.
(52) Perdew, J. P.; Wang, Y. Accurate and simple analytic representation of the electron-gas correlation energy. *Phys. Rev. B: Condens. Matter Mater. Phys.* **1992**, *45* (23), 13244−13249.
(53) Popescu, V.; Zunger, A. Extracting *E* versus *k* effective band structure from supercell calculations on alloys and impurities. *Phys. Rev. B: Condens. Matter Mater. Phys.* **2012**, *85* (8), 085201.
(54) Medeiros, P. V. C.; Stafström, S.; Björk, J. Effects of extrinsic and intrinsic perturbations on the electronic structure of graphene: Retaining an effective primitive cell band structure by band unfolding. *Phys. Rev. B: Condens. Matter Mater. Phys.* **2014**, *89* (4), 041407.
(55) Giussani, A.; Perumal, K.; Hanke, M.; Rodenbach, P.; Riechert, H.; Calarco, R. On the epitaxy of germanium telluride thin films on silicon substrates. *Phys. Status Solidi B* **2012**, *249* (10), 1939−1944.
(56) Park, I.-M.; Jung, J.-K.; Ryu, S.-O.; Choi, K.-J.; Yu, B.-G.; Park, Y.-B.; Han, S. M.; Joo, Y.-C. Thermomechanical properties and mechanical stresses of Ge2Sb2Te5 films in phase-change random access memory. *Thin Solid Films* **2008**, *517* (2), 848−852.
(57) Brandes, E. A., Brook, G. B., Eds. *Smithells Metals Reference Book*; Butterworth-Heinemann: Woburn, MA, 1999.

DOI: 10.1021/acsaelm.9b00596
ACS Appl. Electron. Mater. 2019, 1, 2619−2625